AGU PUBLICATIONS

JGR

Journal of Geophysical Research: Atmospheres

RESEARCH ARTICLE
10.1002/2017JD028219

Key Points:
- The differences in the climatological HC between spring and autumn are mainly derived from their equatorially asymmetric components
- The amplitude of the HC response to different SST meridional structures is much greater in spring than in autumn
- Different ocean variability modes are responsible for the differences in spring and autumn HEA but not for the HES

Correspondence to:
J. Li,
ljp@bnu.edu.cn

Citation:
Feng, J., Li, J., Jin, F.-F., & Zheng, F. (2018). A comparison of the response of the Hadley circulation to different tropical SST meridional structures during the equinox seasons. *Journal of Geophysical Research: Atmospheres*, *123*, 2591–2604. https://doi.org/10.1002/2017JD028219

Received 18 DEC 2017
Accepted 16 FEB 2018
Accepted article online 23 FEB 2018
Published online 9 MAR 2018

A Comparison of the Response of the Hadley Circulation to Different Tropical SST Meridional Structures During the Equinox Seasons

Juan Feng[1], Jianping Li[1,2], Fei-Fei Jin[3], and Fei Zheng[4]

[1]State Key Laboratory of Earth Surface Processes and Resource Ecology and College of Global Change and Earth System Science, Beijing Normal University, Beijing, China, [2]Laboratory for Regional Oceanography and Numerical Modeling, Qingdao National Laboratory for Marine Science and Technology, Qingdao, China, [3]School of Ocean and Earth Science and Technology, University of Hawai'i at Mānoa, Honolulu, Hawaii, [4]State Key Laboratory of Numerical Modeling for Atmospheric Sciences and Geophysical Fluid Dynamics, Institute of Atmospheric Physics, Chinese Academy of Sciences, Beijing, China

Abstract The response of the Hadley circulation (HC) to different tropical sea surface temperature (SST) patterns during the equinox seasons (i.e., boreal spring and autumn) is analyzed. Although the HC shows quasi-equatorially symmetric structure in both equinox seasons, both the climatology and the interannual variations of the HC display considerable differences, that is, being more equatorially asymmetric (symmetric) during autumn (spring). After decomposing the variations of the HC and zonal SST into the equatorially asymmetric (i.e., HC's equatorially asymmetric variation (HEA) for HC and SST's equatorially asymmetric variation (SEA) for SST) and symmetric (i.e., HC's equatorially symmetric variation (HES) for HC and SST's equatorially symmetric variation (SES) for SST) components, the differences in the HC between spring and autumn are shown to derive mainly from the HEA. Meanwhile, the contrast in the response of the HEA to SEA against HES to SES is greater in spring than in autumn, suggesting the HC is more sensitive to the SST conditions in spring. The variation of the HEA is related to different signals in spring and autumn that is linked to the central Pacific El Niño during spring but to the Atlantic Multidecadal Oscillation during autumn. The different contributors are associated with the differences in both the spatial extent and temporal variations in the HEA. In contrast, both spring and autumn HES are closely linked to the canonical El Niño, favoring similar variations in spring and autumn HES. The results here provide a possible explanation of the different variations in the HC during spring and autumn and highlight the seasonal dependence of the response of the HC to SST.

1. Introduction

The Hadley circulation (HC) is a global scale tropical atmospheric meridional circulation, whose ascending and descending branches bridge the tropics and subtropics, significantly influencing the climate at low, middle, and high latitudes (e.g., Chang, 1995; Diaz & Bradley, 2004; Feng et al., 2013). Recently, there has been growing interest in the spatiotemporal variability and width of the HC. Empirical orthogonal function (EOF) analysis of the spatiotemporal variability of the HC has shown that both the seasonal cycle (Dima & Wallace, 2003; Feng, Li, Jin, et al., 2017), long-term annual variability (Feng et al., 2015), and seasonal variability (e.g., Feng et al., 2011, 2013; Guo et al., 2015; Ma & Li, 2008) of the HC are dominated by an equatorially asymmetric mode, with the ascending branch shifted away from the equator. The second mode presents an equatorially symmetric distribution, with the ascending branch around the equator. Similar dominant modes are seen in the month-to-month variations of the HC (Feng, Li, Wang, et al., 2017). Although the HC is dominated by these two distinct modes through the different seasons, the explained variances of the equatorially asymmetric and symmetric modes differ greatly in different seasons. For example, the equatorially asymmetric mode explains more than 50% of the variance during boreal spring (Feng et al., 2013), but only about 30% during boreal autumn (Guo et al., 2015), indicating strong seasonal differences.

Meanwhile, the width of the HC has attracted much attention, because the positions of the ascending and descending branches generally correspond to the tropical convection regions and subtropical semiarid zones, respectively. Based on three reanalysis data sets, Fu et al. (2006) reported that the HC shows evident poleward expansion in each hemisphere over 1979–2005. Subsequently, many other studies have

investigated further the variations in the width of the HC based on different reanalyses and observational data sets, with a focus on its seasonal and annual variations (e.g., Hu & Fu, 2007; Lu et al., 2007; Stachnik & Schumacher, 2011). Despite the differences in the exact magnitude of the expansion, the greater poleward expansion of the HC during the boreal summer and autumn seasons than during the other two seasons in each hemisphere has been confirmed (e.g., Hu & Fu, 2007; Hu et al., 2013; Johanson & Fu, 2009), showing large differences among seasons.

Besides the characteristics of the HC itself, the impacts of the underlying thermal conditions on the variations of the HC have been investigated. The role of the meridional distribution of the tropical sea surface temperature (SST) in the variation of the HC has been intensively discussed. Based on a boundary layer theoretical model, Schneider and Lindzen (1977) showed that the position and strength of the convergence in the boundary layer is related to the meridional structure of tropical SST. Subsequent studies have supported this conclusion and indicated that the ascent in the lower troposphere is related to the meridional distribution of SST (e.g., Lindzen & Nigam, 1987; Hou & Lindzen, 1992). Later, Numaguti (1994) indicated that the convergent flow in the planetary boundary layer is connected to the meridional gradient of SST. Recently, Feng et al. (2013) have demonstrated that the distribution of the meridional gradient of tropical SST determines the structure of the anomalous HC; that is, the position of the meridional maximum of tropical SST corresponds to the location of anomalous ascent (Feng & Li, 2013). That is, the meridional structure of tropical SST determines the distribution of the HC. Moreover, the responses of the HC to different SST meridional structures have different amplitudes even if the magnitude of SST is fixed (Feng et al., 2016; Feng, Li, Jin, et al., 2017). These previous studies have emphasized the importance of the meridional structure of tropical SST on the variations of the HC.

In addition, it has been pointed out that the HC mainly adopts different regimes between the equinox and solstice seasons (Bordoni & Schneider, 2010; Walker & Schneider, 2006). This result is helpful for understanding the seasonal differences of the HC; for example, the different variability of the HC in boreal winter and autumn is due to the different regimes. However, this is not the case for the differences between equinox seasons, such as boreal spring and autumn. In fact, strong seasonal dependence is seen in both the long-term variability and width of the HC. On the other hand, as mentioned above, the response of the HC to SST is sensitive to the meridional structure of tropical SST, and tropical SST displays evident seasonal features (Enfield & Mayer, 1997; Li & Ding, 2013). Therefore, it is of interest to examine whether the response of the HC to tropical SST exhibits seasonal dependence, and if it does show definite seasonal differences, to determine in which season the contrast of the response of the HC to asymmetric and symmetric SST is larger, and to investigate the potential cause of the different response contrasts.

During solstice seasons, the local Rossby number $Ro \rightarrow 1$ in the cross-equatorial winter cell, and $Ro \rightarrow 0$ in the summer cell, indicates that the winter cell mainly adopts angular momentum conserving, while the summer cell is closer to being eddy driven (Schneider & Bordoni, 2008). However, with intermediate *Ro* values during the equinox seasons, there are no theories for the case of intermediate *Ro*, in which nonlinear momentum fluxes associated both with eddies and with the mean circulation are important to the upper branches of the HC (Schneider, 2006; Schneider & Bordoni, 2008; Walker & Schneider, 2006). That is, the theory of the HC during the equinox seasons is not as well understood as during the solstice seasons. In the present study, we will focus on the equinox seasons, that is, boreal spring (March to May) and autumn (September to November), to assess and compare the response contrast of the HC to SST during these two seasons, and to explore the possible causes for their seasonal differences. The remainder of this paper is organized as follows. Data sets and methodology are described in section 2. The response of the HC to different SST meridional structures during boreal spring and autumn is compared in section 3. The possible causes of the differences in the response contrasts of the HC to SST between boreal spring and autumn are outlined in section 4. Finally, section 5 contains a short discussion and our conclusions.

2. Data Sets and Methodology

2.1. Data Sets

Three atmospheric reanalysis data sets were employed to objectively evaluate the characteristics of the HC. These data sets were from the European Centre Medium-Range Weather Forecasts (ECMWF) interim reanalysis (ERAI) globally archived data set on a 1.5° × 1.5° horizontal resolution (Dee et al., 2011), the Japanese 55 year Reanalysis (JRA) on a horizontal resolution of 1.25° × 1.25° (Kobayashi et al., 2015), and the

ECMWF's Atmospheric reanalysis of the twentieth century (ERA-20C; Poli et al., 2016) on a resolution of 2.5° × 2.5°. All reanalyses have 32 vertical levels. The ERA-20C is used to verify the result during a longer period (i.e., 1948–2010). The meridional wind and vertical motion have been used to depict the variation of the HC. The National Centers for Environmental Prediction/National Center for Atmospheric Research (NCEP/NCAR) reanalysis is not employed for that it shows limitation in depicting the variation of the HC. For example, it is reported that the HC associated with NCEP/NCAR is stronger than the observations (Waliser et al., 1999), and NCEP/NCAR reanalysis shows limitation in depicting the seasonal cycle of the equatorially symmetric variations of the HC (Feng, Li, Jin, et al., 2017). Two global SST reanalysis data sets are used to examine the tropical SST features. They are the Extended Reconstructed SST version 3 on a 2° × 2° resolution (Smith et al., 2008) and the UK Met Office Hadley Centre's sea ice and SST data set with a 1° × 1° horizontal resolution (Rayner et al., 2003). The Niño 3 index used to depict the variability of the canonical El Niño–Southern Oscillation is available from https://www.esrl.noaa.gov/psd/gcos_wgsp/Timeseries/Data/, the Atlantic Multidecadal Oscillation index (AMOI) is employed to characterize the variability of the Atlantic Multidecadal Oscillation (AMO) downloaded via https://www.esrl.noaa.gov/psd/data/correlation/, and El Niño–Southern Oscillation Modoki index (EMI; Ashok et al., 2007) is used to indicate the variations of the named date line El Niño (Larkin & Harrison, 2005), El Niño Modoki (EM; Ashok et al., 2007), or the central Pacific El Niño (Yu & Kao, 2007) which is from http://www.jamstec.go.jp/frcgc/research/d1/iod/DATA/. The common available period of 1979–2016 was used in the present study to explore the response characteristics of the HC to tropical SST during boreal spring and autumn. The seasons are based on the Northern Hemisphere (NH), that is, the average of March to May for spring and September to November for autumn in the context. Due to the consistency of the results based on ERAI and JRA, we present results based on ERAI and only point to exceptions when the two data sets disagree.

2.2. Methodology

The HC is characterized by the zonal-mean vertical motion and the mass stream function (MSF). The detailed calculation of the MSF is seen in Feng et al. (2016). To compare the response of the HC to different SST meridional structures during the equinox seasons, the variations of the vertical motion, MSF and zonal-mean SST are linearly decomposed into two components, that is, the equatorially symmetric and asymmetric variations according to Feng, Li, Jin, et al. (2017). The symmetric and asymmetric components of vertical motion and zonal-mean SST (referred as SES and SEA in the context) is obtained by as follows:

$$fs(y) = \frac{f(y) + f(-y)}{2}, \quad fa(y) = \frac{f(y) - f(-y)}{2} \tag{1}$$

In contrast, considering that the values of MSF include both direction and magnitude, the same values of MSF in the Southern Hemisphere (SH) and NH display opposite directions. The equatorially asymmetric and symmetric variations of MSF is defined as follows:

$$\mathrm{HEA}(y) = \frac{\mathrm{MSF}(y) + \mathrm{MSF}(-y)}{2}, \quad \mathrm{HES}(y) = \frac{\mathrm{MSF}(y) - \mathrm{MSF}(-y)}{2}, \tag{2}$$

where y is the meridional locations north of the equator. The details regarding the calculation and schematic illustration are presented in Feng, Li, Jin, et al. (2017).

EOF analysis was employed to obtain the dominate mode of the interannual variability of the equatorially asymmetric and symmetric variations of the seasonal HC and SST. Correlation and regression are used to illustrate the relationships between the SST and HC. Spatial correlation was used to evaluate the similarity of spatial distribution patterns of two variables. The statistical significance of the correlation and regression values was evaluated by means of a two-sided Student's t test.

3. Responses of the HC to SST During Spring and Autumn

3.1. Climatological Characteristics

To assess the response of the HC to the tropical SST during the equinox seasons, the variations of the zonal-mean vertical motion, MSF, and zonal-mean SST are decomposed into two components based on the method presented in section 2. The characteristics of the climatological meridional circulation and tropical SST are first examined. Figure 1 displays the climatological MSF, vertical motion, and their equatorially asymmetric and symmetric variations during boreal spring and autumn in ERAI. Similar features are observed for

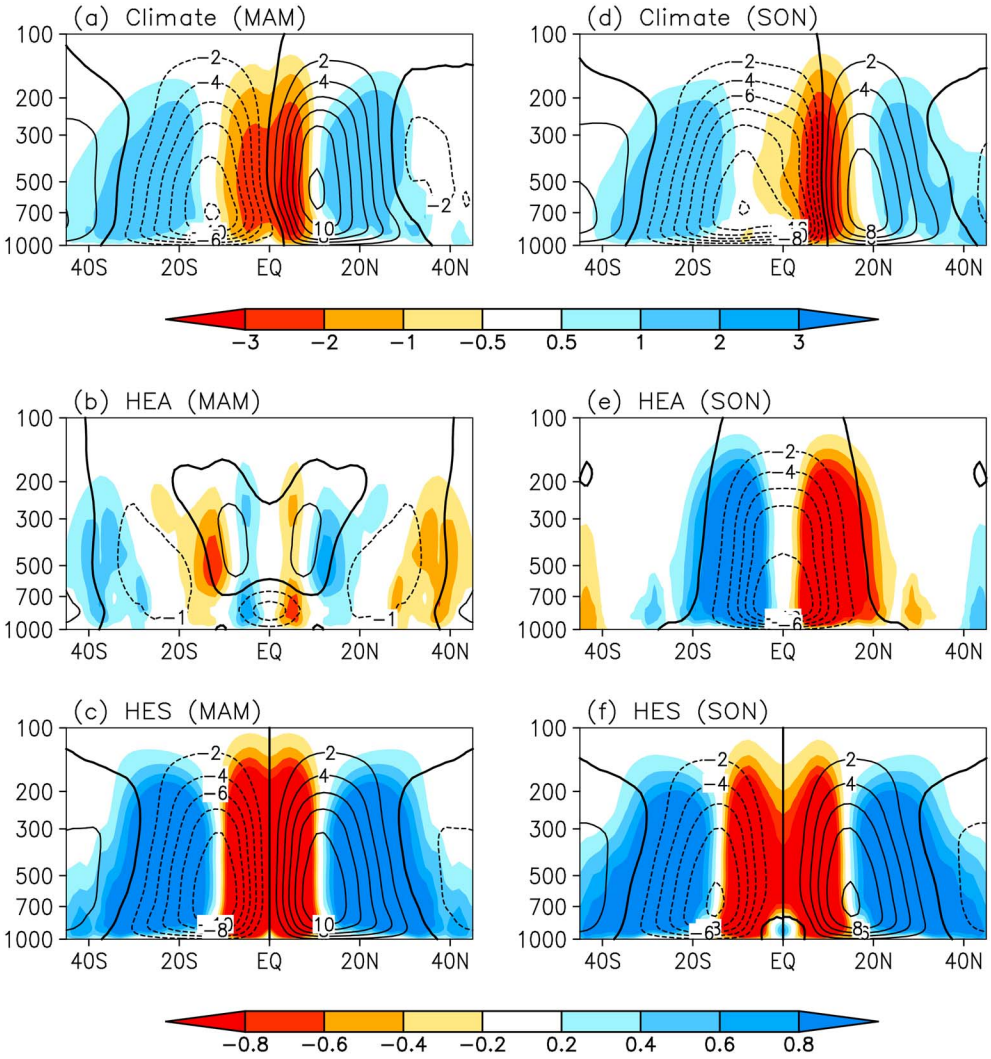

Figure 1. (a) Climatological distribution of the boreal spring mass stream function (contour) and vertical motion (shaded; unit: 10^{-2} P/s). The contour interval is 0.02×10^{10} kg/s. The solid (dotted) contours are positive (negative), zero contour in thickened. (b) and (c) As in (a) but for the equatorially asymmetric and symmetric variations of the mass stream function and vertical motion, respectively. (d–f) As in (a)–(c) but for the distributions during autumn. MAM = March-April-May; SON = September-October-November.

JRA (figures not shown). In spring, an equatorially mirrored meridional circulation is observed, with equivalent extent and magnitude for the northern and southern cells. The combined ascending branch is located around the equator, and the two descending branches are at around 30° latitude in each hemisphere (Figure 1a). The spatial distribution of autumn HC is similar to that during boreal spring, but the intensity and extent of the southern cell are greater than those of the northern counterpart, and the combined ascending branch is located around 10°N rather than around the equator (Figure 1d). This result implies that the equatorially asymmetric variation of the HC in autumn is greater than in spring, which is seen in the climatological distribution of the HEA (Figure 1b versus 1e). The HEA exhibits opposite vertical motion in the tropical NH and SH, that is, ascent to the north of the equator and descent to the south during autumn, but the opposite situation is seen in spring. The HEA during autumn has larger magnitude than during spring, and this is consistently observed in the vertical motion and MSF. In addition, there is a subordinated circulation, that is, ascending around 5°N whereas descending around 5°S in the vertical motion during spring, however, not observed during autumn, suggesting the spatial nonuniformity of the underlying SST during spring. The HES in both spring and autumn contains two equatorially mirrored cells, with the maximum ascent at the equator, and two descending branches in the subtropical regions in each

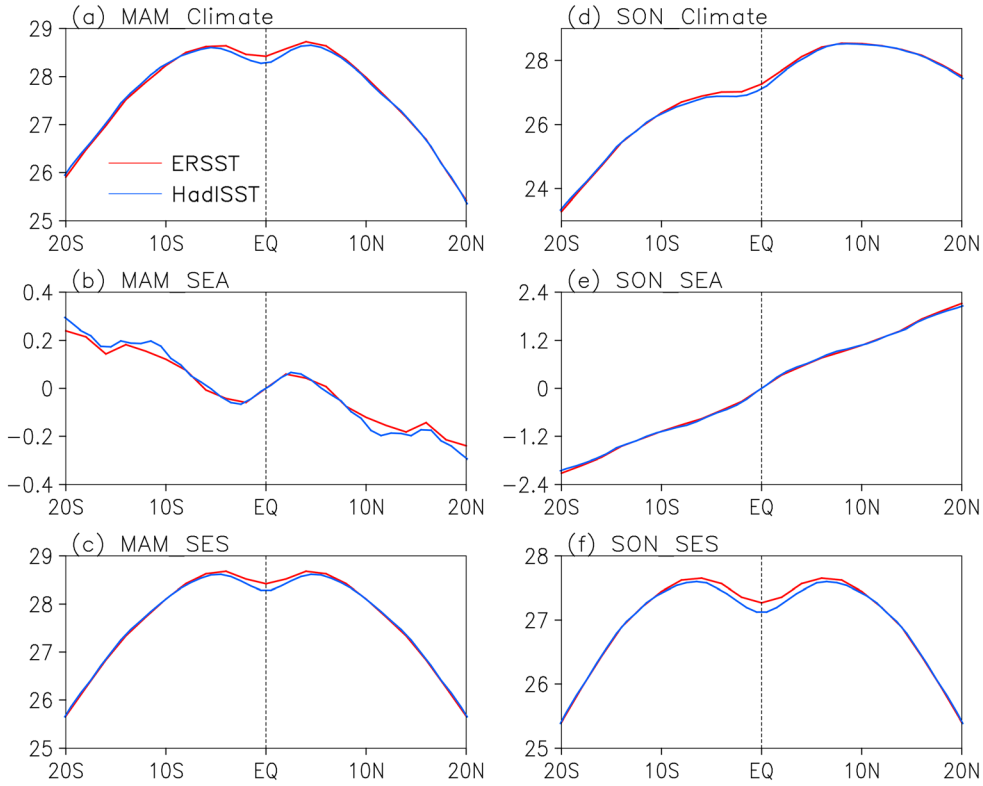

Figure 2. (a) Climatological distribution of boreal spring zonal-mean tropical SST based on Extended Reconstructed Sea Surface Temperature (ERSST) (red) and Hadley Centre sea ice and SST data set (HadISST) (blue) (°C), respectively. (b) and (c) As in (a) but for the equatorially asymmetric and symmetric variations of the zonal-mean SST, respectively. (d–f) As in (a)–(c) but for the distributions during autumn. MAM = March-April-May; SON = September-October-November.

hemisphere. The magnitude of HES during spring is a little stronger than in autumn, but the extent is similar. This result indicates that although the climatological distributions of spring and autumn HC are similar, the equatorially asymmetric variation of the HC during autumn is greater than during spring; in contrast, the equatorially symmetric variation of spring HC is a little stronger than that of autumn HC.

The climatological distribution of the zonal SST, SEA, and SES is displayed in Figure 2. The climatological distribution of the zonal-mean SST is equatorially symmetric during spring, that is, with two equivalent peaks mirrored at the equator (Figure 2a). However, in autumn the peak in the NH has much larger amplitude than that in the SH, and the maximum is around 10°N (Figure 2d), consistent with the position of the maximum ascent of autumn HC. The climatological distribution of tropical SST agrees with the spatial structures of the HC, showing greater equatorially asymmetric variation in autumn than in spring. That is, the difference of the climatological SST between spring and autumn is mainly associated with the SEA component (Figure 2b versus 2e). The SEA during autumn has nearly linear variation, being positive in the NH and negative in the SH. In spring the polarity is reversed, with positive SEA in the SH and negative in the NH, associated with a meridional circulation with ascent in the SH and descent in the NH (Figure 1b). There is also more pronounced variability around the equator in spring, associated with a local weak meridional circulation. Besides, the amplitude of the SEA is around 0.4°C during spring;however, it is ~4°C during autumn. The magnitude of the HEA during spring is ~2×10^8 kg/s, and it is ~10×10^8 kg/s during autumn. This result indicates that response amplitude of the HEA to SEA in the climatology is different between spring and autumn. Unlike the SEA, the distribution of SES is very similar in the two seasons, with peaks mirrored at the equator, although the amplitude in spring is greater than in autumn (Figure 2c versus 2f), in accordance with a much stronger HES during spring as mentioned above.

The above results present the climatological characteristics of the HC and zonal SST, as well as their equatorially asymmetric and symmetric components. More similarities are observed in the equatorially symmetric

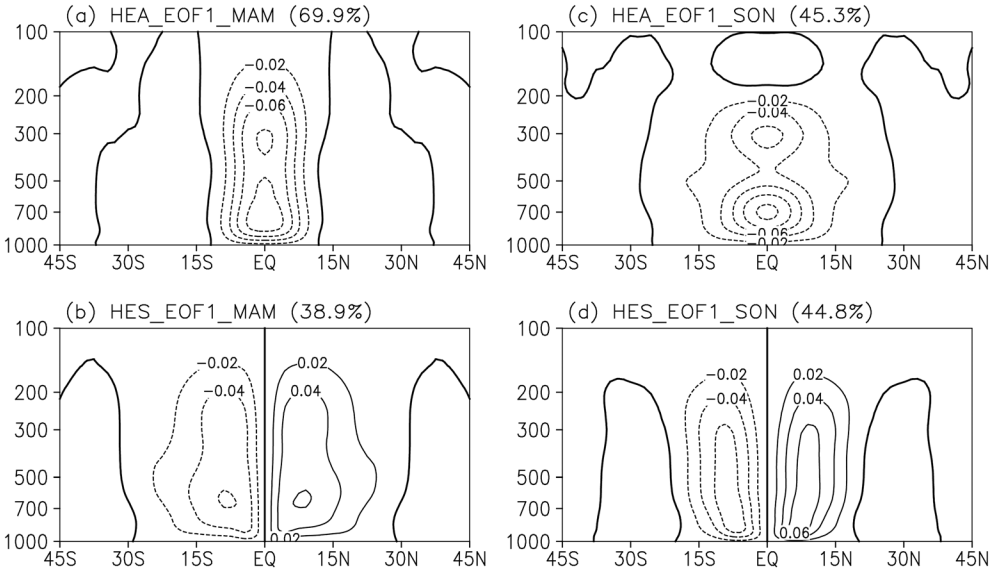

Figure 3. (a) The EOF1 of the equatorially asymmetric variations of the Hadley circulation during spring. The contour interval is 0.02×10^{10}kg/s. The solid (dashed) contours are positive (negative), zero contour is thickened. (b) As in (a) but for the EOF1 of the equatorially symmetric variations of the HC. (c and d) As in (a) and (b) but for the distributions during autumn.

components for both the HC and SST between spring and autumn, while the equatorially asymmetric variations during different seasons are very different. In addition, it is seen that the spatial distribution of the climatological SST determines the distribution of the HC, for both equatorially symmetric and asymmetric variations.

3.2. Interannual Variability

The spatial and temporal variations of spring and autumn HC and zonal SST are illustrated based on the EOFs. The first dominant mode (EOF1) of HEA explains 69.9% of the variance (Figure 3), with an equatorially asymmetric structure during spring, similar to the situation in the annual mean (Feng et al., 2016). The EOF1 of spring HES is equatorially symmetric, with an explained variance of 38.9%. The spatial structures for the EOF1 of HEA and HES during autumn resemble those during spring, but with different extent, that is, broader for the EOF1 of HEA with less explained variance (45.3%) but narrower with equivalent explained variance (44.8%) for the EOF1 of HES. This result indicates that the EOF1s of HES in spring and autumn are highly consistent, and the differences are mainly derived from the EOF1s of the HEA.

Unlike the situation for the HC, both the spatial structures and the explained variances of the EOF1 for the SEA and SES agree closely (Figure 4). For example, the principal mode of SEA is equatorially asymmetric with equivalent amplitude in both spring and autumn, explaining a variance of ~85%. The primary mode of SES has a parabolic structure with the maximum at the equator, explaining a variance of ~88% in both spring and autumn. The principal components of the EOF1 (PC1) for the HC and SST during spring and autumn are shown in Figure 5. There is no evident interdecadal variation in the PC1 of spring HEA and SEA, while the PC1 of autumn HEA and SEA has an evident upward trend. Meanwhile, the PC1 of the HES and SES displays strong interannual variations. The correlation coefficients of the corresponding PC1s are 0.71 (0.53) for HEA against SEA and 0.38 (0.63) for HES against SES during spring (autumn), respectively. These significant correlations confirm that the variations in HES are related to the SES, and the variations in HEA are associated with the SEA as shown in Feng et al. (2016).

In the above we have analyzed the variability of the equatorially symmetric and asymmetric components of the HC and zonal SST. Despite the close relationship between the PC1s of HEA and SEA, and of HES and SES, the consistency between the EOF1 in the SST during spring and autumn cannot explain the differences in the EOF1 of the HC. This is particularly evident for the asymmetric parts, where the EOF1 of the SEA varies similarly in spring and autumn, but the EOF1 of HEA shows obvious differences, suggesting the response of the HC to SST may differ in spring and autumn.

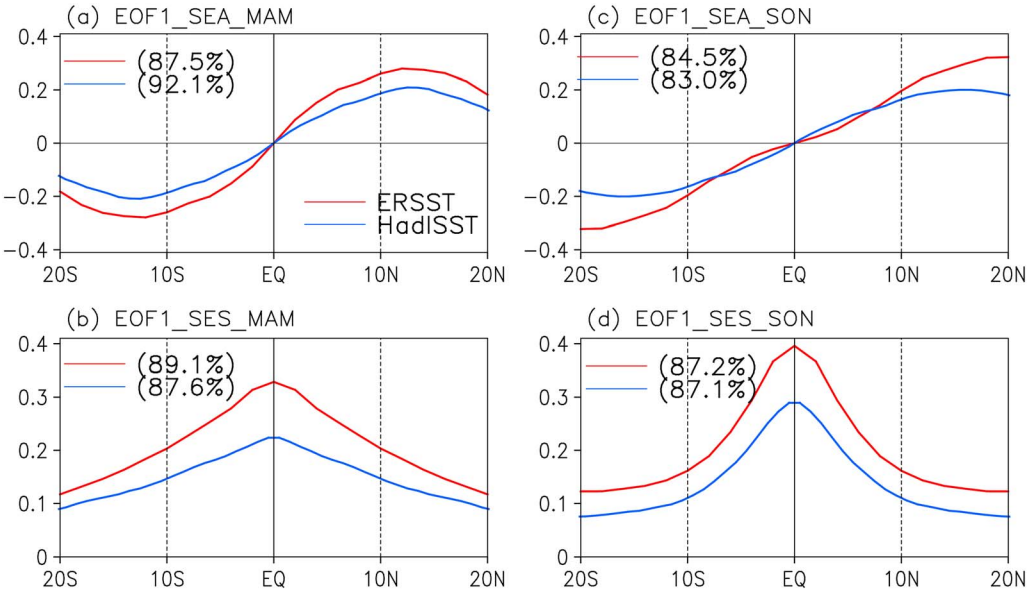

Figure 4. (a) The EOF1 of the equatorially asymmetric variation of zonal sea surface temperature (SST) during spring. (b) As in (a) but for the equatorially symmetric variation of zonal SST. (c and d) As in (a) and (b) but for the distributions during autumn. The red and blue lines indicate based on the Extended Reconstructed Sea Surface Temperature and Hadley Centre clobal sea ice and SST data sets, respectively.

3.3. Response of the HC to SST

Accordingly, the amplitudes of the response of the HEA to SEA, and of the HES to SES, during spring and autumn are analyzed. Figure 6 displays scatterplots of the PC1 of HEA against that of the SEA, and of the PC1 of HES against SES. As well as the significant linear relationships between HEA and SEA, and between HES and SES, we see that the response of HEA to SEA is significantly stronger than that of the HES to SES. For example, a unit variation in the SEA is associated with a 55 (30) unit variation in the HEA during spring (autumn), but the corresponding response of HES to unit variation of SES is a 5 (8) unit variation. Note that the different response of the HEA to SEA during spring and autumn support the amplitude differences of HEA during spring and autumn shown in Figure 1. Moreover, this result shows that the amplitude of the response of HEA to SEA is much larger than that of HES to SES even if the magnitudes of the SST forcing are the same. Consistent results are obtained with different reanalyses as shown in Table 1. Besides the differences in the response amplitude between the HEA and HES to SST, the response contrast of the HEA to SEA

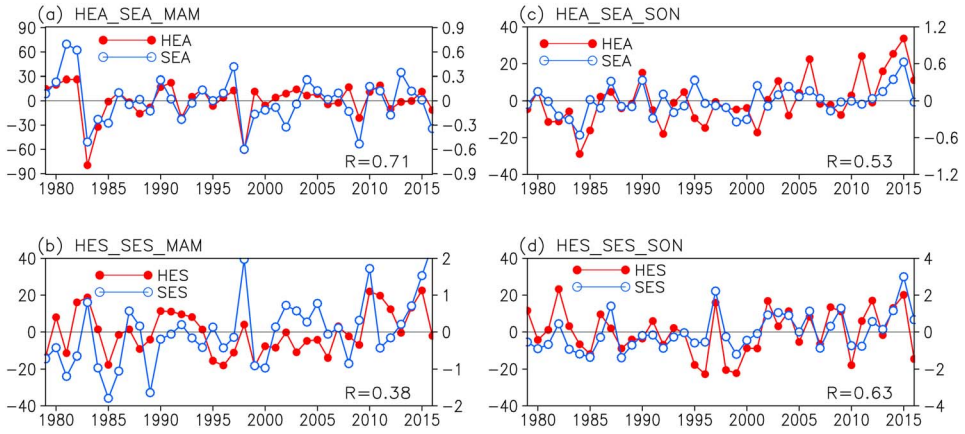

Figure 5. (a) The PC1s of the HEA (red with solid circles) and SEA (blue with open circles) during spring. (b) As in (a) but for the PC1s of the HES and SES. (c and d) As in (a) and (b) but for autumn.

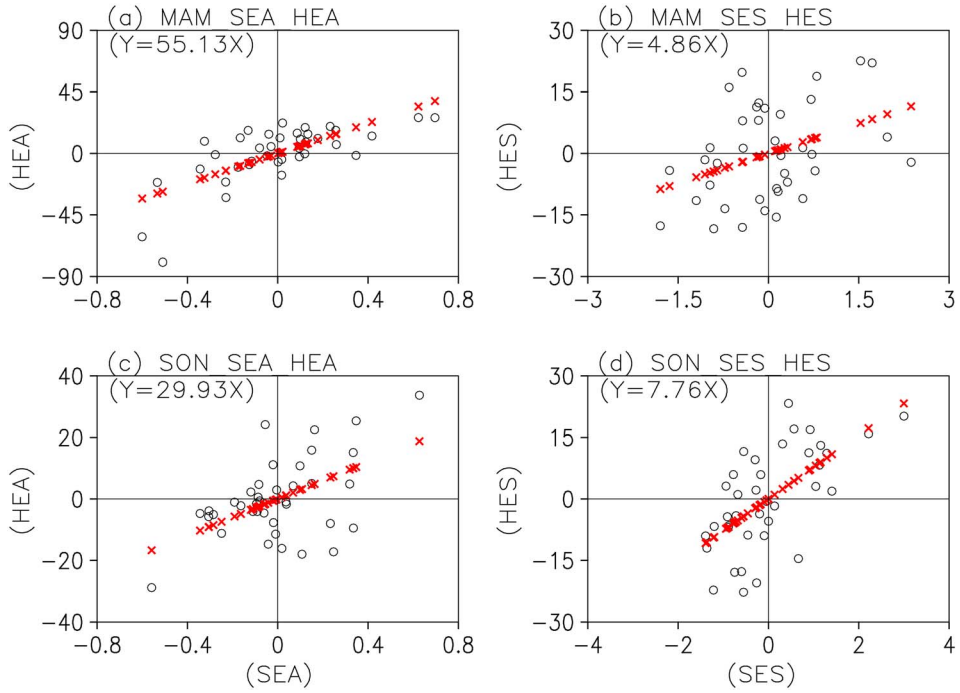

Figure 6. (a) Scatterplot of the PC1s of the SEA against the PC1s of the HEA during spring (black circles) and their linear fit (red crosses). (b) As in (a) but for the scatterplot of the PC1s of the SES against the PC1s of the HES. (c and d) As in (a) and (b) but for autumn.

with respect to that of the HES to SES displays evident differences between spring and autumn. The sensitivity of HEA and HES to SST is around 11 (7) during spring based on ERAI (JRA); however, it is about 4 (3) during autumn as displayed in Table 1. Although different reanalyses give different values of the response amplitudes and ratios, the results are broadly consistent and indicate that (1) the response amplitude of the HEA to SST is at least 3 times larger than that of the HES, which is consistent with previous studies (Feng, Li, Jin, et al., 2017), and (2) the response contrast of the HEA and HES to SST is about twice as strong in spring than in autumn. The result here provides a possible explanation for the greater explained variance of EOF1 for HEA during spring than during autumn, despite the explained variance and magnitude of EOF1 for SEA showing equivalent variations in the spring and autumn. On the other hand, we see that the response contrast of the HC to different SST meridional structures during autumn is closer to the result in the annual mean (Feng et al., 2016) and the seasonal cycle (Feng, Li, Jin, et al., 2017), whereas the response contrast during spring is

Table 1
Regression Coefficients of the PC1 of HEA (HES) With Respect to the PC1 of SEA (SES) and Their Ratio During Spring and Autumn Calculated Using the Various Reanalysis Data Sets

		ERSST			HadISST		
Season	Data Set	ASY	SYM	Ratio	ASY	SYM	Ratio
Spring (MAM)	ERAI	55.13	4.86	11.3	35.84	2.92	12.3
	JRA	76.84	11.38	6.8	48.14	6.95	6.9
	ERA-20C	33.76	2.62	12.9	24.90	2.17	11.5
Autumn (SON)	ERAI	29.93	7.76	3.9	19.87	5.50	3.6
	JRA	35.06	10.41	3.4	22.81	7.09	3.2
	ERA-20C	19.76	5.26	3.8	13.60	4.22	3.2

Note. The European Centre Medium-Range Weather Forecasts (ECWMF) interim reanalysis (ERAI) and Japanese 55 year Reanalysis (JRA) are for the period 1979–2016, and ECWMF's Atmospheric reanalysis of the twentieth century (ERA-20C) is for the period 1948–2010. ERSST = Extended Reconstructed Sea Surface Temperature; HadISST = Hadley Centre sea ice and SST data set; MAM = March-April-May; SON = September-October-November.

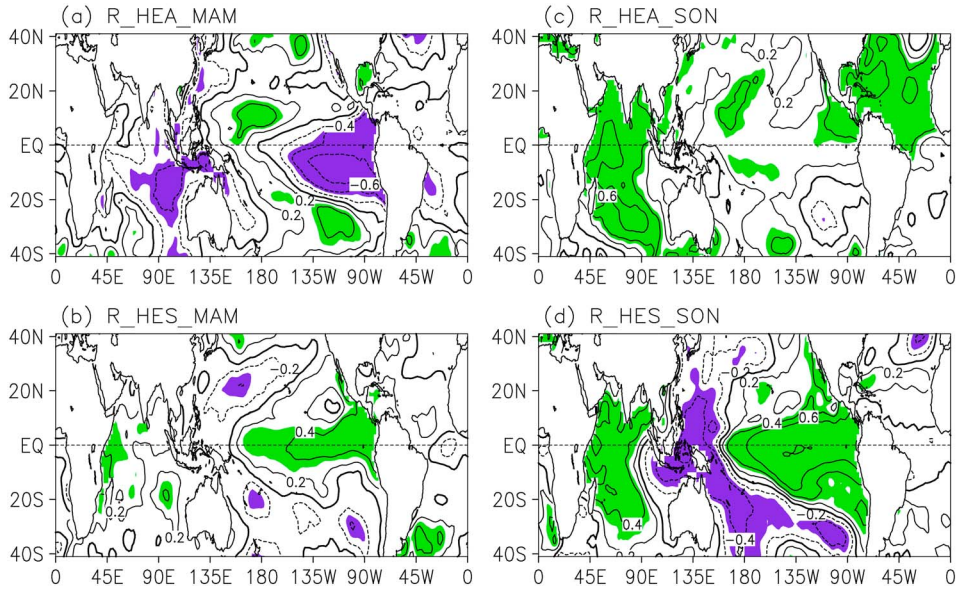

Figure 7. (a) Correlation distribution between the PC1s of the HEA and sea surface temperature during spring. (b) As in (a) but for the correlations between the PC1s of the HES and sea surface temperature. (c and d) As in (a) and (b) but for autumn. Shading indicates significance at the 0.05 level.

much larger, implying that the meridional circulation during spring is more sensitive to the meridional structure of the SST than during autumn. Moreover, there are strong seasonal dependences in the response of the HC to different SST meridional structures even in the same HC regime.

4. Possible Factors Contributing to the Different Response Ratios in Spring and Autumn

The response of the HC to SST is illustrated above, highlighting the greater difference in the response of the HC to different SST meridional structures during spring than during autumn. The possible causes for their different responses are explored in this section. Note that only the correlations between the SST and PC1 of the HEA and HES are shown because the PC1s of the HEA and SEA, and of HES and SES are significantly correlated (as seen in Figure 6). Moreover, significant positive spatial correlation coefficients (beyond 0.60) are obtained between the correlation fields associated with the PC1s of the HEA and SEA, the PC1s of the HES and SES in the SST (figures not shown) within region 40°S–40°N, 0°E–360°E, indicating high agreement in the variations of the HEA and SEA, and HES and SES. The correlation between the SST and PC1 of HEA shows an equatorially asymmetric distribution in both boreal spring and autumn, that is, generally negative in the tropical SH during spring (Figure 7a), while positive correlations dominate in the tropical NH during boreal autumn (Figure 7c). Also, significant negative correlations are seen over the tropical eastern and western Pacific during boreal spring, but with positive correlation over the central Pacific north of the equator (Figure 7a); this spatial distribution of the correlations resembles the pattern known as the date line El Niño (Larkin & Harrison, 2005), El Niño Modoki (Ashok et al., 2007), the central Pacific El Niño (Yu & Kao, 2007), or the warm pool El Niño (Kug et al., 2009) as shown in Figure 8a. This is verified by the significant correlations between the EMI and the PC1s of HEA and SEA with coefficients of 0.46 and 0.47, respectively. The variation of HEA during autumn is associated with significant positive correlations over the northern Atlantic and Indian Ocean, resembling the positive phase of the AMO (Figure 8c). Also, the correlation between the AMOI and PC1 of the HEA (SEA) is 0.53 (0.49), indicating that the variation of HEA (SEA) is connected to the AMO during autumn. As to the relationship between SST and HES, similar spatial distributions are observed in both spring and autumn (Figures 7b and 7d), with stronger signal during autumn. For example, significant positive correlations are found over the eastern Pacific, with negative (positive) correlations over the western Pacific (Indian Ocean). The spatial distributions of the correlations here are similar to the canonical El Niño pattern (Figures 8b and 8d). This explains why more similarities are found in the equatorially symmetric variations

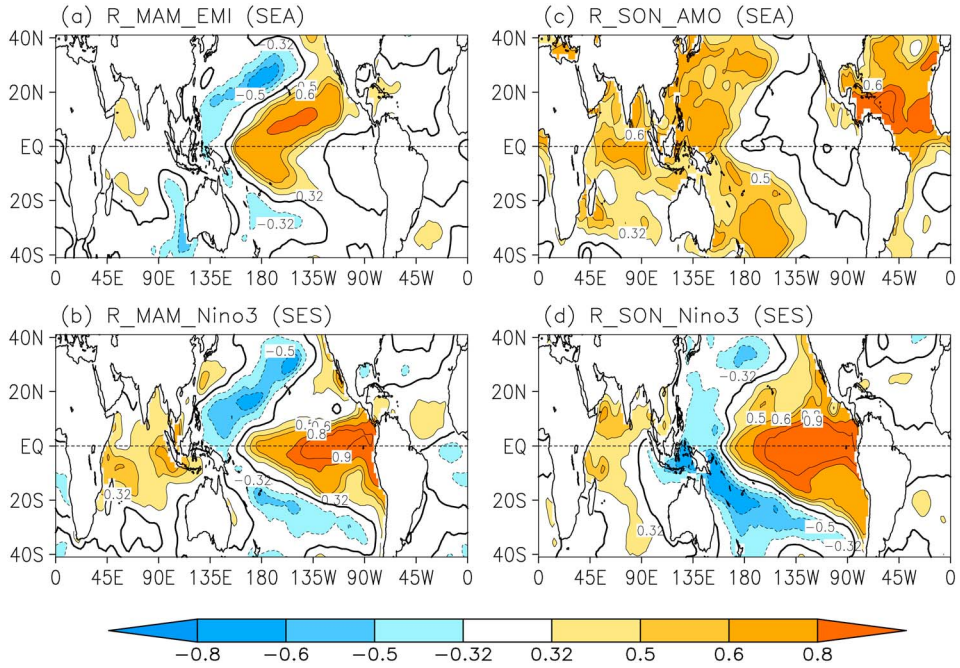

Figure 8. (a) Correlation distribution between the El Niño–Southern Oscillation Modoki index and sea surface temperature (SST) during spring. (b) As in (a) but for the distribution between the Niño 3 index and SST. (c) As in (a) but for the distribution between the AMOI and SST during autumn. (d) As in (b) but for autumn.

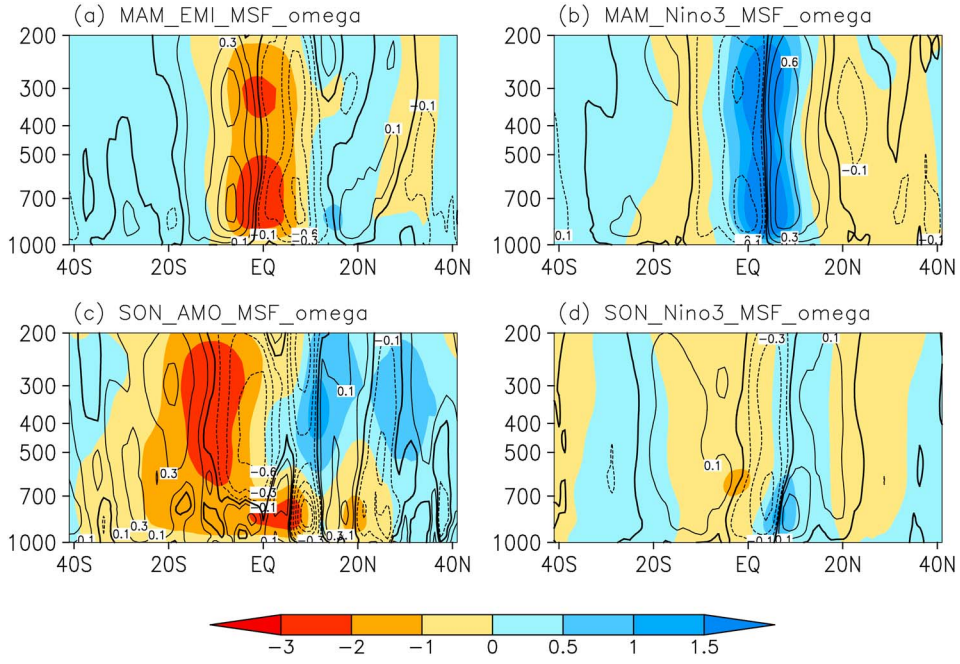

Figure 9. (a) Regression pattern of the mass stream function (MSF) (shaded) and vertical motion (contour) with respect to the El Niño–Southern Oscillation Modoki index (EMI) during spring. (b) As in (a) but for the regression with respect to the Niño 3 index. (c) As in (a), but for the regression with respect to the Atlantic Multidecadal Oscillation index during autumn. (d) As in (b) but for autumn. AMO = Atlantic Multidecadal Oscillation; MAM = March-April-May; SON = September-October-November.

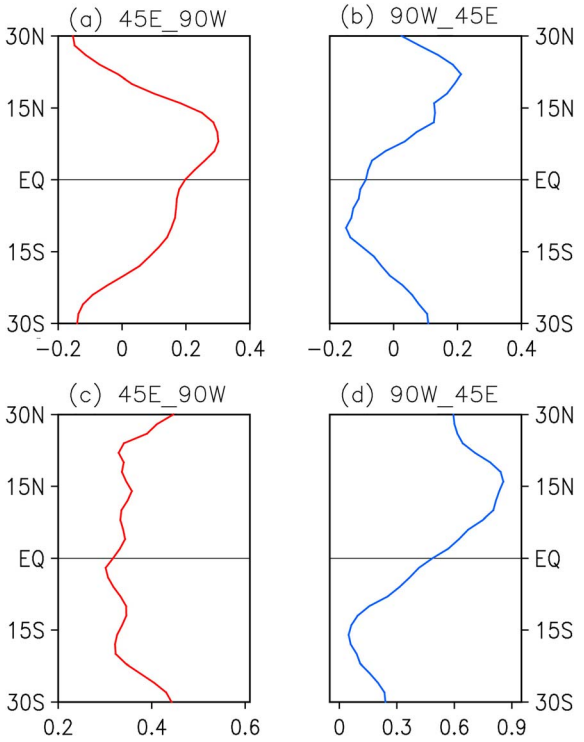

Figure 10. The zonal profiles of the correlations between the El Niño–Southern Oscillation Modoki index and sea surface temperature during boreal spring over 45°E–90°W. (b) As in (a) but over 90°W–45°E. (c and d) As in (a) and (b) but of the correlations between the Atlantic Multidecadal Oscillation index and sea surface temperature during boreal autumn.

of the HC and SST during spring and autumn; they are both associated with the variations of El Niño. In contrast, the HEA (SEA) is related to the EM during spring but to the AMO during autumn.

The possible contributions of the EM, AMO, and El Niño to the meridional circulation are further examined by determining the regressions between the respective indices and the meridional circulation in terms of the zonal-mean vertical motion and MSF, as shown in Figure 9. The regression between the spring EMI and meridional circulation implies an equatorially asymmetric circulation, with the main ascent located in the NH, and descent in the SH, which is consistently observed in both the MSF (shaded) and vertical motion (contours; Figure 9a). This result suggests that the meridional circulation connected with the EM is equatorially asymmetric, demonstrating that the EM favors the variation of the HEA during spring. Similar equatorially asymmetric meridional circulation anomalies are observed associated with the AMO during autumn but with broader meridional extent (Figure 9c). Meanwhile, the variation of El Niño is accompanied by an equatorially symmetric circulation in both spring and autumn, with combined ascent at the equator, and descent in the subtropics in each hemisphere (Figures 9b and 9d).

The above result is consistent with the previous researches on the interannual variability of the seasonal HC. For example, the EM is associated with the equatorially asymmetric SST anomalies during boreal spring (Feng & Li, 2013), the AMO contributes to the temporal variation of the variability of autumn HC (Guo et al., 2015), and the developing and decay phases of El Niño contribute to the variation of HC (Sun & Zhou, 2014). However, unlike in previous studies, we have decomposed variations of the HC into the variations of the equatorially asymmetric and symmetric components that we have examined separately. Our results confirm previous findings and further have outlined the type of spatial variations of the HC linked to the AMO, EM, and El Niño. The results here give a possible explanation of the differences between autumn and spring HC: that it is mainly due to the differing equatorially asymmetric variations derived from different modes of ocean variability.

In addition, the reason why a stronger response of HEA to SST during spring than that during autumn is further explored. It is seen that spring EM related SST pattern displays a more equatorially asymmetric distribution than that associated with autumn AMO (Figure 8). This point is further verified by the zonal-mean profiles of the correlations between the EMI (AMOI) and SST (Figure 10). The global is divided into two ocean basins, that is, Indian-Pacific basin (45°E–90°W) and Atlantic basin (90°W–45°E), due to the correlation features between the EMI (AMOI) and SST. The meridional distribution of correlations between the EMI and SST shows equatorially asymmetric structures in both Indian-Pacific and Atlantic ocean basins that is decreased with decreasing latitudes from 15°N to 15°S. A similar spatial profile is seen for that of AMO but only in Atlantic while showing little meridional change within Indian-Pacific basin. This result indicates that similar equatorially asymmetric distribution in the global SST is associated with the occurrence of EM during boreal spring. However, it is only observed in Atlantic for autumn AMO. Since the meridional circulation is closely linked to the meridional distribution of SST, this result provides a possible explanation for the stronger response of HEA to SST during spring than that during autumn.

5. Discussion and Conclusions

We have examined the variability of the HC during boreal spring and autumn based on two atmospheric reanalyses covering the period 1979–2016. By decomposing the variations of the HC into equatorially asymmetric and symmetric components, the differences in the spatial field of the climatological HC during spring and autumn are shown to be mainly due to the equatorially asymmetric components. The equatorially symmetric variations of the HC are very similar in both climatological extent and intensity during spring and

autumn. The greater importance of the dominant mode of the spring HEA is due to the enhanced response of the HC to different SST meridional structures during spring. That is, a stronger HEA is associated with a given SEA forcing in spring than in autumn, implying that the HC is more sensitive to the underlying thermal conditions during spring than in autumn. In contrast, the response ratio of the HC to asymmetric and symmetric SST during autumn is comparable to that of the annual mean (Feng et al., 2016) and the seasonal cycle (Feng, Li, Jin, et al., 2017), suggesting a strong seasonal dependence in the response of the HC to SST forcing on interannual scales. Consistent result is seen in the period 1948–2010 based on ERA-20C; that is, the ratio of HEA to SEA with respect to HES to SES is ~11 in spring while ~4 in autumn (figure not shown; Table 1), indicating the robustness of the result.

Moreover, we have found that the HEA during spring is significantly associated with the EM, whereas it is connected to the AMO in autumn. The HES is related to El Niño in both spring and autumn. This result provides an explanation for the evident differences between the equatorially asymmetric variation of the HC in spring and autumn; they are controlled by different modes of ocean variability. On the other hand, the AMO exhibits strong interdecadal variations (Enfield & Mestas-Nuñez, 2001), and the PC1 of autumn HEA shows a clear upward trend. In contrast, since the HEA during boreal spring is affected by the EM, there is no obvious trend in the PC1 of the HEA. The EM is predicted to occur more often in the future (Liu et al., 2017), and this may lead to an intensification of the HEA during MAM in the future. It may be interesting to investigate the variation of the HC in simulations of the future scenarios with Coupled Model Intercomparison Project models to further evaluate the variability of the HC.

Furthermore, we have concluded that the equatorially symmetric variations of HC in both spring and autumn are connected to El Niño. However, the standard deviation of the Niño 3 index during autumn is larger than during spring, and this is consistent with our result that the EOF1 of HES in autumn explains greater variance than that in spring. However, it is still unclear why the response contrast of the HC to different SST meridional structures is greater in spring than in autumn. The EM is related with a global uniform equatorially asymmetric distribution in both the Indian-Pacific and Atlantic basins. However, the equatorially asymmetric distribution is only seen in the Atlantic basin in the AMO related SST pattern, which provides a possible explanation for the stronger response of HEA to SEA during spring. In addition, the different contrast in the response of the HC to SST during spring from those seen in the annual mean and seasonal cycle suggests a strong seasonal dependence in the response of the HC to SST. Note that spring is neither a monsoon-dominated season nor in the mature phase of El Niño, when air-sea interactions are particularly strong. Since the seasonal mean is analyzed in this study, it is not feasible to use the lead-lag analysis to show the causality of relationship between the HC and SST. However, as shown in Feng, Li, Jin, et al. (2017), the simultaneous relationship between the HC and SST is most significant, and 1 month leads or lags would not change the response ratio of the HC to SST in the seasonal cycle. Meanwhile, the response of the HC to SST is well reproduced in the theoretical and numerical models during the annual mean (Feng et al., 2016). Note that spring and autumn HC display similar spatial structure with that in annual mean HC, supporting the viewpoint that SST modulate the variation of HC during these seasons. On the other hand, there are some specific behaviors that occur in spring, that is, the spring predictability barrier (e.g., Lau & Yang, 1996, Troup, 1965, Webster & Yang, 1992). It is therefore of interest to further evaluate the possible role of such behavior in determining the response of the HC to SST. The availability of the numerical models provides a possible way to explore this issue and will be discussed in future work. Also, the possible role of background climate conditions in determining the enhanced response contrast during spring merits further investigation. Bearing in mind that the Indo-Pacific warm pool is strongest during boreal spring, it may be interesting to further examine the possible impacts of the warm pool on the response contrast of the HC to different SST meridional structures. In addition, comparing that autumn is generally corresponding to the developing phases of El Niño, while spring could either correspond to the decaying phases or the developing phases of El Niño. This enhances the complexity of the response of the HC to SST during spring.

The present study focuses on the equinox seasons, but the HC during boreal winter and summer exhibits strong interdecadal and interannual variations (Li & Feng, 2017), and the winter and summer cells are dominated by different regimes (Walker & Schneider, 2006). The associated response of the HC to SST during these seasons is still unknown. However, boreal summer is the monsoon season, when the prevailing monsoon circulation dominates the Asia-Australia domain, with strong air-sea feedback. For example, as reported that prevailing of the monsoon could alter adjacent ocean SST via wind-evaporation-SST mechanism (e.g., Ding

& Chan, 2005; Wang et al., 1999). Boreal winter corresponds to the mature phase of El Niño with complex and active air-sea interactions on both regional and global scales. Thus, the circulation and SST during boreal winter and summer show strong regional characteristics and are less zonally uniform than those during spring and autumn. In addition, the calculation of MSF is based on mass conservation and gives a global zonal mean. Therefore, the MSF based on the meridional wind is not suitable for depicting the regional meridional circulation. Some other variables, such as the vertical shear of the meridional wind (Oort & Yienger, 1996) and velocity potential (Tanaka et al., 2004), show limitations in depicting the variations of the HC (Tanaka et al., 2004). Thus, it is difficult to distinguish the role of regional circulation on the response of the HC to SST from the observational data sets. However, sensitivity experiments using coupled simulations provide a feasible approach to assessing the impact of regional air-sea interactions on the response of the HC to SST. Further work on this topic will be carried out to improve understanding of the impacts of regional climatic events on the variation of the HC as well on the regional meridional circulation.

Finally, the equatorially asymmetric variation of spring and autumn HC are connected to different SST signals (i.e., the EM and AMO), but the EM and AMO display different interannual and interdecadal variations, suggesting that different climatic effects may be associated with the variations of HEA during spring and autumn seasons. On the other hand, the developing and decay phases of El Niño also display diverse influences on the regional climate (i.e.,Feng & Li, 2011; Huang & Wu, 1989; Xue & Liu, 2007). Therefore, the decomposition used here provides a feasible approach to separating the individual effects of the equatorially asymmetric and symmetric components of the HC, since these components show different spatial and temporal variations and are controlled by different modes of ocean variability. Further work regarding the climatic effects of the HC on the regional climate using the decomposition method will be carried out to further understand the role of the HC in determining global and regional climatic anomalies, which will be helpful for further understanding the climatic effects of the HC and regional climate change.

Acknowledgments
This work was jointly supported by the SOA Program on Global Change and Air-Sea interactions (GASI-IPOVAI-03) and the National Natural Science Foundation of China (41790474 and 41475076). The ERA-Interim and ERA-20C reanalyses were obtained from http://apps.ecmwf.int/datasets/. The JRA reanalysis is available online at http://jra.kishou.go.jp/JRA-55/index_en.html. The ERSST reanalyses were obtained from NOAA and are available at http://www.esrl.noaa.gov/psd/data/gridded/. The HadISST data set was obtained from the UK Met Office Hadley Centre and is available online at http://www.metoffice.gov.uk/hadobs/hadisst/data/download.html.

References

Ashok, K., Behera, S. K., Rao, S. A., Weng, H., & Yamagata, T. (2007). El Niño Modoki and its possible teleconnection. *Journal of Geophysical Research*, *112*, C11007. https://doi.org/10.1029/2006JC003798

Bordoni, S., & Schneider, T. (2010). Regime transitions of steady and time-dependent Hadley circulations: Comparison of axisymmetric and eddy-permitting simulations. *Journal of the Atmospheric Sciences*, *67*(5), 1643–1654. https://doi.org/10.1175/2009JAS3294.1

Chang, E. K. M. (1995). The influence of Hadley circulation intensity changes on extratropical climate in an idealized model. *Journal of the Atmospheric Sciences*, *52*(11), 2006–2024. https://doi.org/10.1175/1520-0469(1995)052%3C2006:TIOHCI%3E2.0.CO;2

Dee, D. P., Uppala, S. M., Simmons, A. J., Berrisford, P., Poli, P., Kobayashi, S., et al. (2011). The ERA-Interim reanalysis: Configuration and performance of the data assimilation system. *Quarterly Journal of the Royal Meteorological Society*, *137*(656), 553–597. https://doi.org/10.1002/qj.828

Diaz, H. F., & Bradley, B. (2004). *The Hadley circulation: Present, past and future*. Netherlands: Kluwer Academic Publishers. https://doi.org/10.1007/978-1-4020-2944-8

Dima, I. M., & Wallace, J. M. (2003). On the seasonality of the Hadley cell. *Journal of the Atmospheric Sciences*, *60*(12), 1522–1527. https://doi.org/10.1175/1520-0469(2003)060%3C1522:OTSOTH%3E2.0.CO;2

Ding, Y. H., & Chan, J. C. L. (2005). The East Asian summer monsoon: An overview. *Meteorology and Atmospheric Physics*, *89*, 117–142.

Enfield, D. B., & Mayer, D. A. (1997). Tropical Atlantic sea surface temperature variability and its relation to El Niño-Southern Oscillation. *Journal of Geophysical Research*, *102*(C1), 929–945. https://doi.org/10.1029/96JC03296

Enfield, D. B., & Mestas-Nuñez, A. M. (2001). The Atlantic Multidecadal Oscillation and its relations to rainfall and river flows in the continental U.S. *Geophysical Research Letters*, *28*(10), 2077–2080. https://doi.org/10.1029/2000GL012745

Feng, J., & Li, J. P. (2011). Influence of El Niño Modoki on spring rainfall over south China. *Journal of Geophysical Research*, *116*, D13102. https://doi.org/10.1029/2010JD015160

Feng, J., & Li, J. P. (2013). Contrasting impacts of two types of ENSO on the boreal spring Hadley circulation. *Journal of Climate*, *26*(13), 4773–4789. https://doi.org/10.1175/JCLI-D-12-00298.1

Feng, J., Li, J., Jin, F., Liu, Z., Nan, X., & Guo, Y. (2016). Contrasting responses of the Hadley circulation to equatorially asymmetric and symmetric meridional sea surface temperature structures. *Journal of Climate*, *29*(24), 8949–8963. https://doi.org/10.1175/JCLI-D-16-0171.1

Feng, J., Li, J. P., Jin, F., Zhao, S., & Xie, F. (2017). The responses of the Hadley circulation to different meridional SST structures in the seasonal cycle. *Journal of Geophysical Research: Atmospheres*, *122*, 7785–7799. https://doi.org/10.1002/2017JD026953

Feng, R., Li, J. P., & Wang, J. C. (2011). Regime change of the boreal summer Hadley circulation and its connection with the tropical SST. *Journal of Climate*, *24*(15), 3867–3877. https://doi.org/10.1175/2011JCLI3959.1

Feng, J., Li, J. P., Wang, Y. Q., & Zhu, J. L. (2017). Decreased response contrast of Hadley circulation to the different meridional structures of tropical sea surface temperature during the recent hiatus. *SOLA*, *13*, 181–185. https://doi.org/10.2151/sola.2017-033

Feng, J., Li, J. P., & Xie, F. (2013). Long-term variation of the principal mode of boreal spring Hadley circulation linked to SST over the Indo-Pacific warm pool. *Journal of Climate*, *26*(2), 532–544. https://doi.org/10.1175/JCLI-D-12-00066.1

Feng, J., Li, J., Zhu, J., Li, F., & Sun, C. (2015). Simulation of the equatorially asymmetric mode of the Hadley circulation in CMIP5 models. *Advances in Atmospheric Sciences*, *32*(8), 1129–1142. https://doi.org/10.1007/s00376-015-4157-0

Fu, Q., Johanson, C. M., Wallace, J. M., & Reichler, T. (2006). Enhanced mid-latitude tropospheric warming in satellite measurements. *Science*, *312*(5777), 1179. https://doi.org/10.1126/science.1125566

Guo, Y. P., Li, J. P., Feng, J., Xie, F., Sun, C., & Zheng, J. (2015). The multidecadal variability of the asymmetric mode of the boreal autumn Hadley circulation and its link to the Atlantic Multidecadal Oscillation. *Journal of Climate*, *29*, 5625–5641.

Hou, A. Y., & Lindzen, R. S. (1992). The influence of concentrated heating on the Hadley circulation. *Journal of the Atmospheric Sciences*, *49*(14), 1233–1241. https://doi.org/10.1175/1520-0469(1992)049%3C1233:TIOCHO%3E2.0.CO;2

Hu, Y. Y., & Fu, Q. (2007). Observed poleward expansion of the Hadley circulation since 1979. *Atmospheric Chemistry and Physics*, *7*(19), 5229–5236. https://doi.org/10.5194/acp-7-5229-2007

Hu, Y. Y., Tao, L. J., & Liu, J. P. (2013). Poleward expansion of the Hadley circulation in CMIP5 simulations. *Advances in Atmospheric Sciences*, *30*(3), 790–795. https://doi.org/10.1007/s00376-012-2187-4

Huang, R. H., & Wu, Y. F. (1989). The influence of ENSO on the summer climate change in China and its mechanism. *Advances in Atmospheric Sciences*, *6*(1), 21–32.

Johanson, C., & Fu, Q. (2009). Hadley cell widening: Model simulations versus observations. *Journal of Climate*, *22*(10), 2713–2725. https://doi.org/10.1175/2008JCLI2620.1

Kobayashi, S., Ota, Y., Harada, Y., Ebita, A., Moriya, M., Onoda, H., et al. (2015). The JRA-55 Reanalysis: General specifications and basic characteristics. *Journal of the Meteorological Society of Japan*, *93*(1), 5–48. https://doi.org/10.2151/jmsj.2015-001

Kug, J. S., Jin, F.-F., & An, S. I. (2009). Two types of El Niño events: Cold tongue El Niño and warm pool El Niño. *Journal of Climate*, *22*(6), 1499–1515. https://doi.org/10.1175/2008JCLI2624.1

Larkin, N. K., & Harrison, D. E. (2005). On the definition of El Niño and associated seasonal average U.S. weather anomalies. *Geophysical Research Letters*, *32*(13), L13705. https://doi.org/10.1029/2005GL022738

Lau, K. M., & Yang, S. (1996). The Asian monsoon and predictability of the tropical ocean-atmosphere system. *Quarterly Journal of the Royal Meteorological Society*, *122*, 945–957.

Li, J. P., & Ding, R. Q. (2013). Temporal-spatial distribution of the predictability limit of monthly sea surface temperature in the global oceans. *International Journal of Climatology*, *33*(8), 1936–1947. https://doi.org/10.1002/joc.3562

Li, J. P., & Feng, J. (2017). In C. B. Fu & H. T. Mao (Eds.), *Tropical large-scale atmospheric interaction in association with subtropical aridity trend: Aridity trend in Northern China* (p. 320). Cambridge: World Scientific Publishing Co Pte Ltd.

Lindzen, R. S., & Nigam, S. (1987). On the role of sea surface temperature gradients in forcing low-level winds and convergence in the tropics. *Journal of the Atmospheric Sciences*, *44*(17), 2418–2436. https://doi.org/10.1175/1520-0469(1987)044%3C2418:OTROSS%3E2.0.CO;2

Liu, Y., Cobb, K. M., Song, H., Li, Q., Li, C. Y., Nakatsuka, T., et al. (2017). Recent enhancement of central Pacific El Niño variability relative to last eight centuries. *Nature Communications*, *8*, 15386. https://doi.org/10.1038/ncomms15386

Lu, J., Vecchi, G. A., & Reichler, T. (2007). Expansion of the Hadley cell under global warming. *Geophysical Research Letters*, *34*, L06805. https://doi.org/10.1029/2006GL028443

Ma, J., & Li, J. P. (2008). The principal modes of variability of the boreal winter Hadley cell. *Geophysical Research Letters*, *35*(1), L01808. https://doi.org/10.1029/2007GL031883

Numaguti, A. (1994). Dynamics and energy balance of the Hadley circulation and the tropical precipitaton zones. Part II: Sensitivity to meridional SST distribution. *Journal of the Atmospheric Sciences*, *52*(8), 1128–1141.

Oort, A. H., & Yienger, J. J. (1996). Observed interannual variability in the Hadley circulation and its connection to ENSO. *Journal of Climate*, *9*(11), 2751–2767. https://doi.org/10.1175/1520-0442(1996)009%3C2751:OIVITH%3E2.0.CO;2

Poli, P., Hersbach, H., & Dee, D. P. (2016). ERA-20C: An atmospheric reanalysis of the twentieth century. *Journal of Climate*, *29*(11), 4083–4097. https://doi.org/10.1175/JCLI-D-15-0556.1

Rayner, N. A., Parker, D. E., Horton, E. B., Folland, C. K., Alexander, L. V., Rowell, D. P., et al. (2003). Global analyses of sea surface temperature, sea ice, and night marine air temperature since the late nineteenth century. *Journal of Geophysical Research*, *108*(D14), 4407. https://doi.org/10.1029/2002JD002670

Schneider, T. (2006). The general circulation of the atmosphere. *Annual Review of Earth and Planetary Sciences*, *34*(1), 655–688. https://doi.org/10.1146/annurev.earth.34.031405.125144

Schneider, T., & Bordoni, S. (2008). Eddy-mediated regime transitions in the seasonal cycle of a Hadley circulation and implications for monsoon dynamics. *Journal of the Atmospheric Sciences*, *65*(3), 915–934. https://doi.org/10.1175/2007JAS2415.1

Schneider, E., & Lindzen, R. S. (1977). Axially symmetric steady state models of the basic state of instability and climate studies. Part I: Linearized calculations. *Journal of the Atmospheric Sciences*, *34*, 253–279.

Smith, T. M., Reynolds, R. W., Peterson, T. C., & Lawrimore, J. (2008). Improvements to NOAA's historical merged land-ocean surface temperature analysis (1880–2006). *Journal of Climate*, *21*(10), 2283–2296. https://doi.org/10.1175/2007JCLI2100.1

Stachnik, J. P., & Schumacher, C. (2011). A comparison of the Hadley circulation in modern reanalyses. *Journal of Geophysical Research*, *116*, D22102. https://doi.org/10.1029/2011JD016677

Sun, Y., & Zhou, T. J. (2014). How does El Niño affect the interannual variability of the boreal summer Hadley circulation? *Journal of Climate*, *27*(7), 2622–2642. https://doi.org/10.1175/JCLI-D-13-00277.1

Tanaka, H. L., Ishizaki, N., & Kitoh, A. (2004). Trend and interannual variability of Walker, monsoon and Hadley circulations defined by velocity potential in the upper troposphere. *Tellus A*, *56*(3), 250–269. https://doi.org/10.3402/tellusa.v56i3.14410

Troup, A. J. (1965). The "southern oscillation". *Quarterly Journal of the Royal Meteorological Society*, *91*(390), 490–506. https://doi.org/10.1002/qj.49709139009

Waliser, D. E., Shi, A., Lanzante, J. R., & Oort, A. H. (1999). The Hadley circulation: Assessing NCEP/NCAR reanalysis and sparse in-situ estimates. *Climate Dynamics*, *15*(10), 719–735. https://doi.org/10.1007/s003820050312

Walker, C. C., & Schneider, T. (2006). Eddy influences on Hadley circulations: Simulations with an idealized GCM. *Journal of the Atmospheric Sciences*, *63*(12), 3333–3350. https://doi.org/10.1175/JAS3821.1

Wang, C. Z., Weisberg, R. H., & Yang, H. J. (1999). Effects of the wind speed-evaporation-SST feedback on the El Niño-Southern Oscillation. *Journal of the Atmospheric Sciences*, *56*(10), 1391–1403. https://doi.org/10.1175/1520-0469(1999)056%3C1391:EOTWSE%3E2.0.CO;2

Webster, P. J., & Yang, S. (1992). Monsoon and ENSO: Selectively interactive systems. *Quarterly Journal of the Royal Meteorological Society*, *118*(507), 877–926. https://doi.org/10.1002/qj.49711850705

Xue, F., & Liu, C. Z. (2007). The influence of moderate ENSO on summer rainfall in eastern China and its comparison with strong ENSO [in Chinese]. *Chinese Science Bulletin*, *53*(5), 791–800.

Yu, J. Y., & Kao, H. K. (2007). Decadal changes of ENSO persistence barrier in SST and ocean heat content indices: 1958–2001. *Journal of Geophysical Research*, *112*, D13106. https://doi.org/10.1029/2006JD007654